Ipomoeassin-F inhibits the *in vitro* biogenesis of the SARS-CoV-2 spike protein and its host cell membrane receptor

Sarah O'Keefe[1,4], Peristera Roboti[1], Kwabena B. Duah[2], Guanghui Zong[3], Hayden Schneider[2], Wei Q. Shi[2] and Stephen High[1,4]

[1]School of Biological Sciences, Faculty of Biology, Medicine and Health, University of Manchester, Manchester, M13 9PT, United Kingdom

[2]Department of Chemistry, Ball State University, Muncie, Indiana 47306, USA

[3]Department of Chemistry and Biochemistry, University of Maryland, College Park, Maryland 20742, USA

[4]Lead Contacts for correspondence: sarah.okeefe@manchester.ac.uk; stephen.high@manchester.ac.uk

Keywords

Cell-free translation, Endoplasmic reticulum (ER), ER membrane complex (EMC), Sec61 translocon, viral protein biogenesis.

Abstract

In order to produce proteins essential for their propagation, many pathogenic human viruses, including SARS-CoV-2 the causative agent of COVID-19 respiratory disease, commandeer host biosynthetic machineries and mechanisms. Three major structural proteins, the spike, envelope and membrane proteins, are amongst several SARS-CoV-2 components synthesised at the endoplasmic reticulum (ER) of infected human cells prior to the assembly of new viral particles. Hence, the inhibition of membrane protein synthesis at the ER is an attractive strategy for reducing the pathogenicity of SARS-CoV-2 and other obligate viral pathogens. Using an *in vitro* system, we demonstrate that the small molecule inhibitor ipomoeassin F (Ipom-F) potently blocks the Sec61-mediated ER membrane translocation/insertion of three therapeutic protein targets for SARS-CoV-2 infection; the viral spike and ORF8 proteins together with angiotensin-converting enzyme 2, the host cell plasma membrane receptor. Our findings highlight the potential for using ER protein translocation inhibitors such as Ipom-F as host-targeting, broad-spectrum, antiviral agents.

Introduction

Viruses are obligate parasites that require host cell machineries to support their cellular invasion, genomic replication and the synthesis of viral progeny. Inhibition of the host factors that are co-opted during viral infection thus provides a powerful strategy for the development of broad-spectrum antiviral agents; a current global need given the paucity of clinically effective antiviral drugs and the emergence of highly pathogenic human viruses (Adalja and Inglesby, 2019).

Many of these viruses, including the causative agent of COVID-19 respiratory disease, SARS-CoV-2 (Zhou et al., 2020; Zhu et al., 2020) (Fig. 1A), hijack the mechanisms of host secretory pathway-mediated protein synthesis in order to correctly synthesise, fold and assemble important viral proteins (Bojkova et al., 2020; Gordon et al., 2020; Sicari et al., 2020). Hence, small molecule inhibitors of Sec61-mediated co-translational protein entry into the endoplasmic reticulum (ER) (Luesch and Paavilainen, 2020) have recently attracted attention as potentially broad-spectrum antiviral agents (Heaton et al., 2016; Shah et al., 2018). Such inhibitors offer a dual approach to reduce viral pathogenicity; first, by directly inhibiting the production of key viral proteins and, second, by reducing the levels of host proteins that are co-opted during viral infection. In the latter case, human angiotensin-converting enzyme 2 (ACE2) is one of the host cell receptors crucial for SARS-CoV-2 viral entry and infectivity (Cantuti-Castelvetri et al., 2020; Daly et al., 2020; Walls et al, 2020). As an integral membrane protein, ACE2 is synthesised at the ER prior to its trafficking to the plasma membrane (Warner et al., 2005), and is thus a potential candidate for down-regulation using inhibitors of ER entry.

Our recent studies show that ipomoeassin-F (Ipom-F) (Fig. 1B) is a potent and selective inhibitor of Sec61-mediated protein translocation into and across the ER membrane (Zong et al., 2019; O'Keefe et al., 2020 submitted). Given that SARS-CoV-2 membrane proteins likely co-opt host mechanisms of ER entry during their biogenesis (cf. Gordon et al., 2020; Sicari et al., 2020), we concluded that their sensitivity to Ipom-F would likely be comparable to that of endogenous Sec61 clients (Fig. 1C; see also Zong et al., 2019; O'Keefe et al., 2020 submitted). We, therefore, evaluated the effects of Ipom-F on a small panel of SARS-CoV-2 proteins that each contain hydrophobic ER targeting signals (Fig. 1D). The *in vitro* membrane insertion

of the viral spike (S) protein and membrane translocation of the ORF8 protein are both strongly inhibited by Ipom-F, whilst several other viral membrane proteins are unaffected (Fig. 2). Likewise, the ER membrane integration of ACE2, an important host receptor for SARS-CoV-2 (Walls et al., 2020), is highly sensitive to Ipom-F (Fig. 2).

We show that the principle molecular basis for the Ipom-F sensitivity of these SARS-CoV-2 proteins is driven by their dependence on the Sec61 translocation complex, as dictated by their individual structural features and membrane topologies (Fig. 3). Taken together, our *in vitro* study of SARS-CoV-2 protein synthesis at the ER highlights Ipom-F as a promising candidate for the development of a broad-spectrum, host-targeting, antiviral agent.

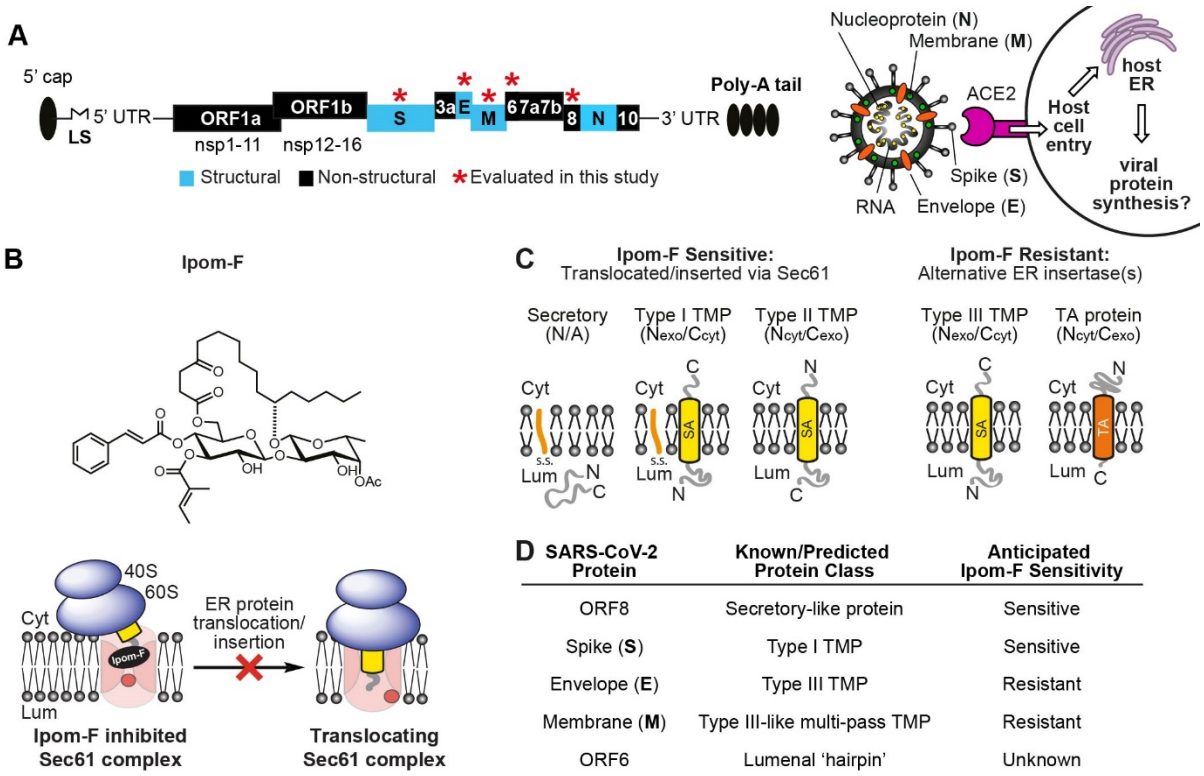

Fig. 1. Ipom-F as a potential inhibitor of SARS-CoV-2 viral protein synthesis. (A) A schematic of the (+) ssRNA genome architecture of SARS-CoV-2 (29903 nt) which contains a 5' capped mRNA with a leader sequence (LS), a 3' end poly-A tail, a 5' and 3' UTR and the open reading frames (ORFs) ORF1a, ORF1b, spike (S), ORF3a, envelope (E), membrane (M), ORF6, ORF7, ORF8, nucleoprotein (N) and ORF10 (Firth, 2020; Naqvi et al., 2020). An important mode of SARS-CoV-2 host entry proceeds via interaction of the viral S protein with human angiotensin-converting enzyme 2 (ACE2) (Walls et al., 2020). (**B**) The chemical structure of Ipomoeassin-F (Ipom-F), a small molecule inhibitor of Sec61-mediated protein translocation into the endoplasmic reticulum (ER). (**C**) Ipom-F efficiently blocks the ER membrane translocation of secretory proteins and the ER insertion of single-pass type I and

90 type II TMPs, but not the insertion of type III TMPs or tail-anchored (TA) proteins. In the
91 schematic, SA denotes a signal anchor. (**D**) Based on the known/predicted membrane
92 topology of candidate SARS-CoV-2 proteins and the sensitivity of comparable host cell
93 proteins (Zong et al., 2019; O'Keefe et al., 2020 submitted), we anticipated their likely
94 sensitivity to an Ipom-F-induced blockade of ER protein translocation.

95 **Results and Discussion**

96 Ipom-F selectively inhibits ER translocation of the viral ORF8 and S proteins

97 In order to explore the ability of Ipom-F to inhibit the ER translocation of a small, yet
98 structurally diverse, panel of SARS-CoV-2 membrane and secretory-like proteins, we
99 first used a well-established *in vitro* translation system supplemented with canine
100 pancreatic microsomes (Fig. 2A). To facilitate the detection of ER translocation, we
101 modified the viral ORF8, S, E, M and ORF6 proteins by adding an OPG2-tag; an
102 epitope that supports efficient ER lumenal N-glycosylation and enables product
103 recovery via immunoprecipitation, without affecting Ipom-F sensitivity of the substrate
104 (Fig. S1A) (O'Keefe et al., 2020 submitted). The identity of the resulting N-glycosylated
105 species for each of these OPG2-tagged viral proteins was confirmed by
106 endoglycosidase H (Endo H) treatment of the radiolabelled products associated with
107 the membrane fraction prior to SDS-PAGE (Fig. 2B, cf. lanes 1 and 2 in each panel).
108

109 Using ER lumenal modification of either endogenous N-glycosylation sites (viral S and
110 M proteins) or the appended OPG2-tag (viral E and ORF8 proteins) as a robust
111 reporter for ER membrane translocation, we found that 1 μM Ipom-F strongly inhibited
112 both the translocation of the soluble, secretory-like protein ORF8-OPG2 and the
113 integration of the type I transmembrane proteins (TMP) S-OPG2, and various
114 truncated derivatives thereof (Fig. 2B, Fig. 2C, Fig. S1C). Furthermore, membrane
115 insertion of the human type I TMP, ACE2, was inhibited to a similar extent (Fig. 2B,
116 Fig. 2C, ~70 to ~90% inhibition for these three proteins). These results mirror previous
117 findings showing that precursor proteins that bear N-terminal signal peptides, and are
118 thus obligate clients for the Sec61-translocon, are typically very sensitive to Ipom-F-
119 mediated inhibition (Zong et al., 2019; O'Keefe et al., 2020 submitted). In the context
120 of SARS-CoV-2 infection, wherein ACE2 acts as an important host cell receptor for
121 the SARS-CoV-2 virus via its interaction with the viral S protein (Walls et al., 2020),
122 these data suggest that an Ipom-F-induced antiviral effect might be achieved via
123 selective reductions in the biogenesis of both host and viral proteins alike (cf. Fig. 1A).

124 In contrast to the viral S and ORF8 proteins, insertion of the viral E protein was
125 unaffected by Ipom-F (Fig. 2B-C), consistent with its recently reported classification as
126 a type III TMP (Duart et al., 2020). Hence, the integration of type III TMPs is highly
127 resistant to Ipom-F (Zong et al., 2019), most likely because they exploit a novel
128 pathway for ER membrane insertion (cf. Fig. 3; O'Keefe et al., 2020 submitted). We
129 therefore conclude that the known substrate-selective inhibitory action of Ipom-F at
130 the Sec61 translocon is directly applicable to viral membrane proteins; whereby the
131 ER translocation of secretory proteins and type I TMPs, but not type III TMPs, is
132 efficiently blocked by Ipom-F. It seems likely that viral type II TMPs will also be inhibited
133 by Ipom-F (cf. Morel et al., 2018; Zong et al., 2019; Gérard et al., 2020) but, since
134 SARS-CoV-2 has no such proteins, we have not addressed this issue.
135
136 The viral M protein is a multi-pass TMP with its first TMD oriented so the N-terminus
137 is exoplasmic (N_{exo}) and hence can be considered "type III-like". Although human
138 multi-pass TMPs of this type typically require both the ER membrane complex (EMC)
139 and Sec61 translocon for their authentic ER insertion (Chitwood et al., 2018), Ipom-F
140 had no significant effect on the ER translocation of the N-terminal domain of the M
141 protein *in vitro* (Fig. 2C). We conclude that the integration of its first TMD is unaffected
142 by Ipom-F, consistent with its use of the EMC (Chitwood et al., 2018; O'Keefe et al.,
143 2020 submitted). Although we cannot rule out any Ipom-F-induced defects in the
144 Sec61-dependent integration of the second/third TM-spans of the M protein (cf.
145 Chitwood et al., 2018), previous studies have shown that similar host cell multi-pass
146 TMPs are resistant to comparable Sec61 inhibitors such as mycolactone (Morel et al.,
147 2018). In practice, the potential resistance of this highly abundant and functionally
148 diverse class of endogenous membrane proteins (von Heijne, 2007) may limit any
149 Ipom-F-induced cytotoxicity towards host cells.

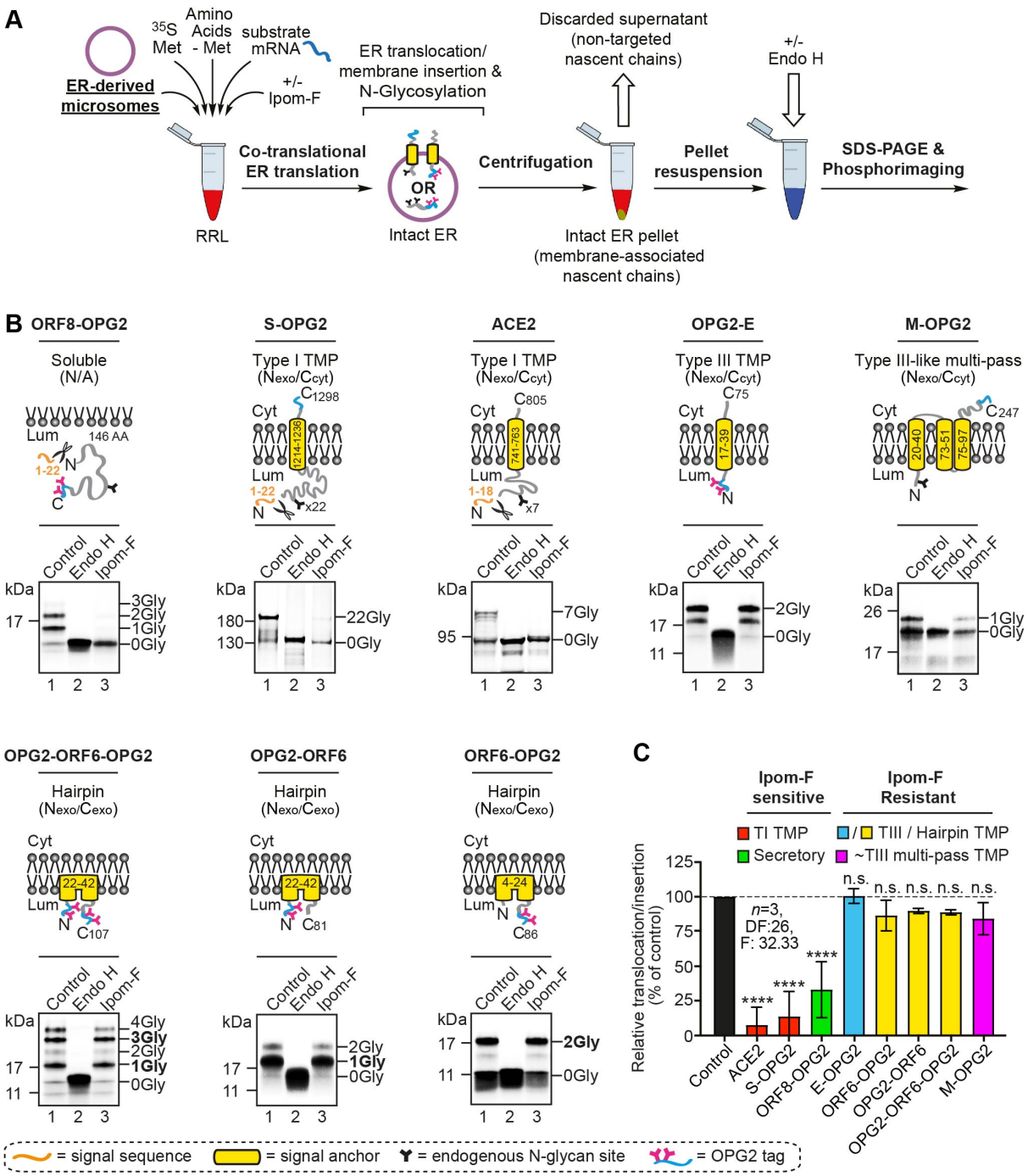

Fig. 2. Ipom-F selectively inhibits the ER membrane translocation of SARS-CoV-2 proteins. (A) Schematic of the *in vitro* ER import assay in which canine pancreatic microsomes are used as a source of ER membrane. Following translation, fully translocated or membrane inserted radiolabelled precursor proteins are recovered with the ER membrane fraction and analysed by SDS-PAGE and phosphorimaging. The identity of N-glycosylated species was confirmed by treatment with endoglycosidase H (Endo H). **(B)** Protein precursors of the human angiotensin-converting enzyme 2 (ACE2) and OPG2-tagged versions of the SARS-CoV-2 ORF8 (ORF8-OPG2), spike (S-OPG2), envelope (OPG2-E), membrane (M-OPG2) and ORF6 (a doubly-OPG2 tagged version, OPG2-ORF6-OPG2, and two singly-OPG2 tagged forms, OPG2-ORF6 and ORF6-OPG2, with their respective predominant N-glycan species highlighted in bold) were synthesised in rabbit reticulocyte lysate

161 supplemented with ER-derived microsomes in the absence or presence of Ipom-F (lanes 1
162 and 3). Phosphorimages of membrane-associated products resolved by SDS-PAGE, together
163 with representative substrate outlines, are shown. N-glycosylation was used as a read-out for
164 the efficiency of membrane translocation/insertion and N-glycosylated (X-Gly) versus non-N-
165 glycosylated (0Gly) species were identified by treatment with Endo H (see lane 2). **(C)** The
166 relative efficiency of membrane translocation/insertion in the presence of Ipom-F was
167 calculated using the ratio of N-glycosylated protein to non-glycosylated protein, relative to the
168 DMSO treated control (set to 100% efficiency). Quantifications are given as means ±SEM for
169 independent translation reactions performed in triplicate (*n*=3) and statistical significance (one-
170 way ANOVA, DF and F values shown in the figure) was determined using Dunnett's multiple
171 comparisons test. Statistical significance is given as n.s., non-significant >0.1; ****, P < 0.0001.

172 <u>ORF6 assumes a lumenal-facing hairpin topology in ER-derived microsomes</u>

173 Cell-based studies of the ORF6 protein from SARS-CoV-1 suggest it has an unusual
174 hairpin topology with both its N- and C-termini located on the exoplasmic side of the
175 host cell membrane, to which it binds via an N-terminal amphipathic helix (Netland et
176 al., 2007). To independently determine the membrane topology of SARS-CoV-2
177 ORF6, we prepared versions with OPG2 tags at both its N- and C-termini, or single
178 tagged equivalents (see Fig. 2B, schematics, OPG2-ORF6-OPG2, OPG2-ORF6 and
179 ORF6-OPG2). Following membrane insertion, doubly tagged OPG2-ORF6-OPG2
180 shows significant amounts of species with 3- and 4-N-linked glycans (Fig. 2B). This
181 pattern confirms that the SARS-CoV-2 ORF6 protein assumes a 'hairpin' conformation
182 in the ER membrane with both its N- and C-termini in the lumen (Fig. 2B, OPG2-ORF6-
183 OPG2). These 3- and 4-N-glycan bearing OPG2-ORF6-OPG2 species are also
184 resistant to extraction with alkaline sodium carbonate buffer (Fig. S1D) and protected
185 from added protease (Fig. S1E), further indicating that the majority of the ORF6 protein
186 is stably associated with the ER membrane in a 'hairpin' (N_{exo}/C_{exo}) topology.
187
188 Consistent with this unusual membrane topology, we find no indication that the
189 membrane insertion of any of our OPG2-tagged ORF6 variants is reduced by Ipom-F,
190 strongly suggesting that its association with the inner leaflet of the ER membrane does
191 not require protein translocation via the central channel of the Sec61 translocon
192 (Gérard et al., 2020; O'Keefe et al., 2020 submitted). We noted a sub-set of OPG2-
193 ORF6-OPG2 species bearing only a single N-glycan was also clearly present in the
194 membrane-associated fraction with or without Ipom-F treatment (Fig. 2B, OPG2-
195 ORF6-OPG2, see 1Gly). Based on comparison to singly OPG2-tagged variants (Fig.
196 2B), we conclude that OPG2-ORF6-OPG2-1Gly has its N-terminus in the ER lumen,

197 where only one of its two consensus sites is efficiently N-glycosylated (cf. Nilsson and
198 von Heijne, 1993), whilst its C-terminus is either ER luminal but non-glycosylated or
199 remains on the cytosolic side of the membrane. In the latter case, it may be that, in
200 addition to its hairpin topology, some fraction of ORF6 may be integrated into ER-
201 derived microsomes as a type III TMP (cf. Fig. S2E; see also Netland et al., 2007) that
202 is resistant to Ipom-F inhibition (this study; Zong et al., 2019; O'Keefe et al., 2020
203 submitted).
204
205 The molecular basis for SARS-CoV-2 protein sensitivity to Ipom-F
206 Having ascertained that Ipom-F inhibits the ER membrane translocation/insertion of
207 the viral ORF8 and S proteins, but not of the ORF6, E or M proteins (Fig. 2C), we next
208 investigated the molecular basis for this selectivity. For these studies we employed
209 semi-permeabilised (SP) mammalian cells, depleted of specific membrane
210 components via siRNA-mediated knockdown, as our source of ER membrane (Fig.
211 3A; Wilson et al., 2007). Consistent with our recent work (O'Keefe et al., 2020
212 submitted), and based on the quantitative immunoblotting of target and control gene
213 products (Fig. S2A-C), we selectively depleted HeLa cells for core components of the
214 Sec61 translocon (Sec61α-kd, ~65% reduction), the EMC (EMC5-kd, ~73% reduction)
215 and both together (Sec61α+EMC5-kd, ~68% and ~78% reduction) prior to semi-
216 permeabilisation with digitonin and use for *in vitro* ER translocation assays.
217
218 Following the analysis of total OPG2-tagged translation products recovered by
219 immunoprecipitation, we found that: i) the S protein and a truncated derivative were
220 both more strongly affected by the depletion of Sec61α than of EMC5 (Fig. 3B, Fig.
221 S2D); ii) the ORF8 protein was likewise strongly affected by Sec61α depletion but also
222 sensitive to EMC5 depletion (Fig. 3C); iii) the E protein showed diminished insertion
223 efficiency after knock-down of Sec61α and EMC5, although the latter had a more
224 pronounced effect (Fig. 3D). In each case, the combined knockdown of Sec61α and
225 EMC5 resulted in a reduction of membrane insertion that was either comparable to, or
226 greater than, that achieved following the knock-down of Sec61α alone (Figs. 3B to
227 3D). For the ORF6 protein, the total level of N-glycosylated OPG2-ORF6-OPG2
228 species was unaffected by any knockdown condition tested (Fig. 3E). However, we
229 note a marked increase in the proportion of potentially mis-inserted OPG2-ORF6-

230 OPG2-1Gly species, particularly after co-depletion of EMC5 and Sec61α (see Fig. 3E;
231 Fig. S2E). We speculate that the unusual hairpin topology of the ORF6 protein may
232 be attributed to the EMC and Sec61 complex acting in concert to provide an Ipom-F
233 insensitive pathway for protein translocation across the ER membrane (O'Keefe et al.,
234 2020, submitted). Perturbation of this pathway seemingly increases the potential for
235 ORF6 to mis-insert (cf. Chitwood et al., 2018), perhaps as a consequence of disruption
236 to the translocation of its C-terminus (Fig. S2E).
237
238 Taken together, our data establish that, analogous to human membrane and secretory
239 proteins, the principal molecular basis for the Ipom-F-sensitivity of the SARS-CoV-2
240 ORF8 and S proteins is their dependence on Sec61-mediated protein translocation
241 into and across the ER membrane. In contrast, the E, M, and ORF6 proteins appear
242 capable of exploiting one or more alternative membrane insertion/translocation
243 pathways that can bypass the translocase activity of the Sec61 complex. These
244 alternatives most likely include a recently described route for type III TMP insertion
245 that requires the insertase function of the EMC (O'Keefe et al., 2020 submitted), which
246 our data suggest is also sufficient to confer Ipom-F-resistance to the viral E protein
247 and at least the first TM-span of the viral M protein.
248
249 Concluding Remarks
250 We conclude, that Sec61-selective protein translocation inhibitors like Ipom-F hold
251 promise as broad-spectrum antivirals that may exert a therapeutic effect by selectively
252 inhibiting the ER translocation of viral and/or host proteins which are crucial to viral
253 infection and propagation (Mast et al., 2020). In the context of SARS-CoV-2,
254 integration of the viral S protein and its host cell receptor, ACE2, into the ER
255 membrane is significantly reduced by Ipom-F (Fig. 2C, 3B). Likewise, translocation of
256 the viral ORF8 protein across the ER membrane and into its lumen is substantially
257 diminished (Fig. 2C, 3C). The binding of the viral S protein to cell surface ACE2 is a
258 key step in host cell infection (Drew and Janes, 2020), whilst ORF8 may protect SARS-
259 CoV-2 infected cells against host cytotoxic T lymphocytes (Zhang et al., 2020), making
260 all three of these proteins viable therapeutic targets (Drew and Janes, 2020; Li et al.,
261 2020; Young et al., 2020). Given that Ipom-F is a potent inhibitor of Sec61-mediated
262 protein translocation in cell culture models (Zong et al., 2019) and appears well
263 tolerated in mice (Zong et al., in press), we propose that future studies investigating

its effect on SARS-CoV-2 infection and propagation in cellular models are clearly warranted.

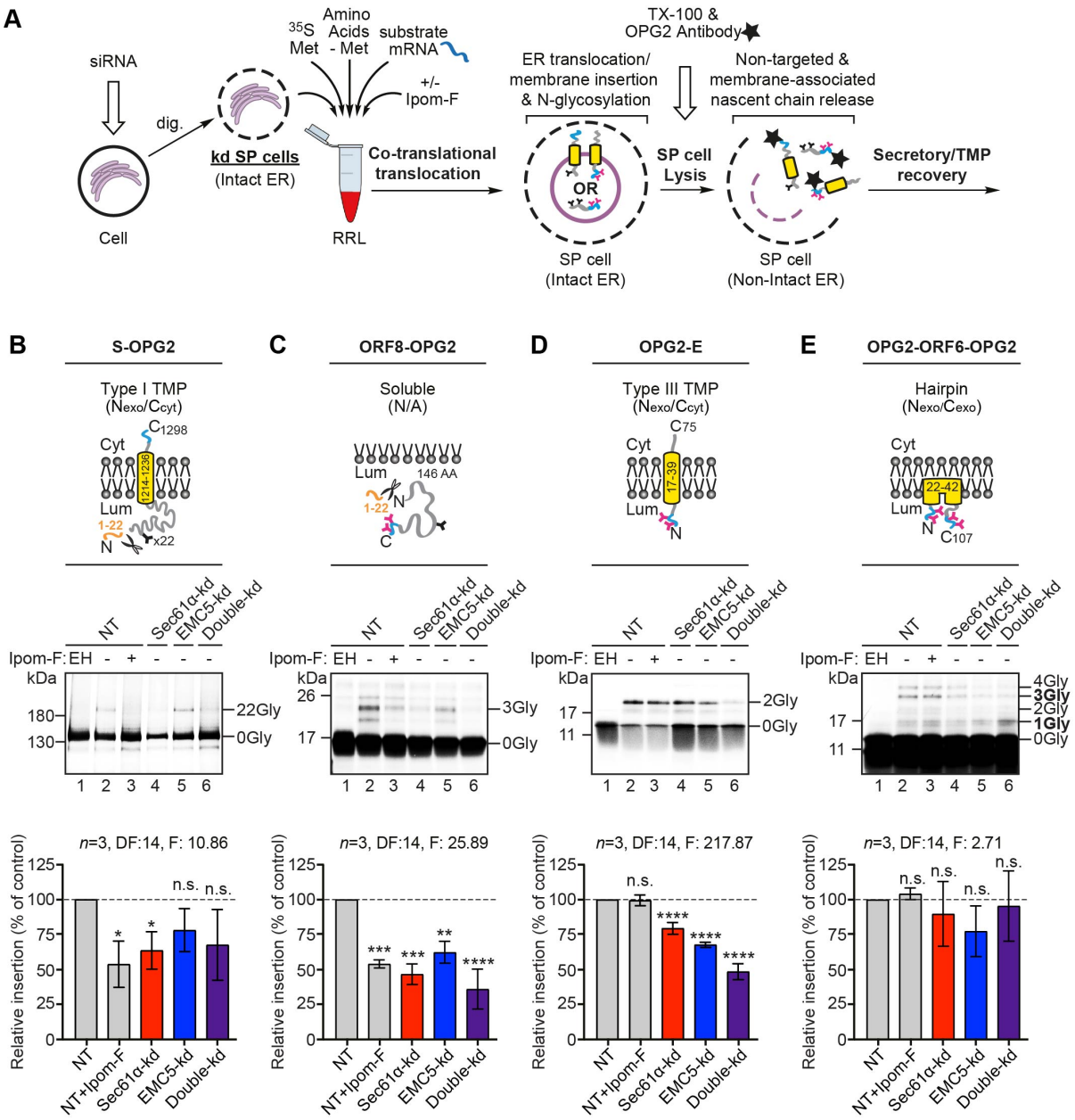

Fig. 3: SARS-CoV-2 proteins are variably dependent on the Sec61 complex and/or the EMC for ER membrane translocation/insertion. (A) Schematic of the *in vitro* ER import assay in which control SP cells, or those depleted of a subunit of the Sec61 complex and/or the EMC via siRNA, are used as a source of ER membrane. Following translation, OPG2-tagged translation products (i.e. membrane-associated and non-targeted nascent chains) are recovered by immunoprecipitation, resolved by SDS-PAGE and analysed by phosphorimaging. OPG2-tagged variants of the SARS-CoV-2 **(B)** spike (S-OPG2), **(C)** ORF8 (ORF8-OPG2), **(D)** envelope (OPG2-E) and **(E)** ORF6 (OPG2-ORF6-OPG2, different Gly species labelled as described in the legend to Fig. 2) proteins were synthesised in rabbit reticulocyte lysate supplemented with control SP cells (lanes 1-2) or those with impaired Sec61 complex and/or EMC function (lanes 3-6). Radiolabelled products were recovered and

277 analysed as described in **(A)**. Membrane translocation/insertion efficiency was determined
278 using the ratio of the N-glycosylation of lumenal domains, identified by treatment with Endo H
279 (EH, lane 1), relative to the NT control (set to 100% translocation/insertion efficiency).
280 Quantifications are given as means ±SEM for independent translation reactions from separate
281 siRNA treatments performed in triplicate (*n*=3) and statistical significance (two-way ANOVA,
282 DF and F values shown in the figure) was determined using Dunnett's multiple comparisons
283 test. Statistical significance is given as: n.s., non-significant >0.1; *, P < 0.05; **, P < 0.01; ***,
284 P < 0.001; ****, P < 0.0001.

285 **Materials and Methods**

286 Ipom-F and Antibodies

287 Ipom-F was synthesised as previously described (Zong et al., in press). Antibodies
288 used to validate Sec61 and/or EMC subunit depletions in SP cells (Fig. S2) were
289 purchased from Santa Cruz Biotechnology (goat polyclonal anti-LMNB1 (clone M-20,
290 sc-6217), Bethyl Laboratories (rabbit polyclonal anti-EMC5 (A305-832-A)), Abcam
291 (rabbit polyclonal anti-EMC6, (ab84902)), gifted by Sven Lang and Richard
292 Zimmerman (University of Saarland, Homburg, Germany, rabbit anti-Sec61α) or as
293 previously described (mouse monoclonal anti-OPG2 tag (McKenna et al., 2016) and
294 rabbit polyclonal anti-OST48 (Wilson et al., 2007).

295

296 DNA constructs

297 The cDNA for human ACE2 (Uniprot: Q9BYF1) was purchased from Sino Biological
298 (HG10108-M). cDNAs encoding the SARS-CoV-2 genes for ORF6, ORF8 and the E
299 M and S proteins (Uniprot: P0DTC6, P0DTC8, P0DTC4, P0DTC5, P0DTC2
300 respectively) were kindly provided by Nevan Krogan (UCSF, US) (Gordon et al. 2020),
301 amplified by PCR, subcloned into the pcDNA5 vector and constructs validated by DNA
302 sequencing (GATC, Eurofins Genomics). ORF6-OPG2, ORF8-OPG2, M-OPG2 and
303 S-OPG2 were generated by inserting the respective cDNAs in frame between NheI
304 and AflII sites of a pcDNA5/FRT/V5-His vector (Invitrogen) containing a C-terminal
305 OPG2 tag (MNGTEGPNFYVPFSNKTG). OPG2-E was generated by cloning the
306 cDNA encoding the E-protein into the same pcDNA5-OPG2 vector using the KpnI and
307 BamHI sites and deleting the stop codon after the OPG2 tag by site-directed
308 mutagenesis (Stratagene QuikChange, Agilent Technologies). The N-terminal OPG2-
309 tag of OPG2-ORF6-OPG2 was inserted by site-directed mutagenesis of ORF6-OPG2
310 using the relevant forward and reverse primers (Integrated DNA Technologies). Linear
311 DNA templates were generated by PCR and mRNA transcribed using T7 polymerase.

312

313 siRNA-mediated knockdown and SP cell preparation

314 HeLa cells (human epithelial cervix carcinoma cells, ATCC, female) were cultured in
315 DMEM supplemented with 10% (v/v) FBS and maintained in a 5% CO_2 humidified
316 incubator at 37°C. Knockdown of target genes were performed as previously
317 described (O'Keefe et al., 2020 submitted) using 20 nM (final concentration) of either
318 control siRNA (ON-TARGETplus Non-targeting control pool; Dharmacon), *SEC61A1*

319 siRNA (Sec61α-kd, GE Healthcare, sequence AACACUGAAAUGUCUACGUUUUU),
320 *MMGT1* siRNA (EMC5-kd, ThermoFisher Scientific, s41129) and INTERFERin
321 (Polyplus, 409-10) as described by the manufacturer. 96 h post-initial transfection,
322 cells were semi-permeabilsed using 80 µg/mL high purity digitonin (Calbiochem) and
323 treated with 0.2 U Nuclease S7 Micrococcal nuclease from *Staphylococcus aureus*
324 (Sigma-Aldrich, 10107921001) as previously described (O'Keefe et al., 2020
325 submitted; Wilson et al., 2007). SP cells lacking endogenous mRNA were
326 resuspended ($3x10^6$ SP cells/mL as determined by trypan blue (Sigma-Aldrich, T8154)
327 staining) in KHM buffer (110 mM KOAc, 2 mM $Mg(OAc)_2$, 20 mM HEPES-KOH pH
328 7.2) prior to analysis by western blot, or inclusion in translation master mixes such that
329 each translation reaction contained $2x10^5$ cells/mL.
330
331 <u>*In vitro* ER import assays</u>
332 Standard translation and membrane translocation/insertion assays, supplemented
333 with nuclease-treated canine pancreatic microsomes (from stock with OD_{280} = 44/mL)
334 or siRNA-treated SP HeLa cells, were performed in nuclease-treated rabbit
335 reticulocyte lysate (Promega) as previously described (Zong et al., 2019; O'Keefe et
336 al., 2020 submitted): namely in the presence of EasyTag EXPRESS ^{35}S Protein
337 Labelling Mix containing [^{35}S] methionine (Perkin Elmer) (0.533 MBq; 30.15
338 TBq/mmol), 25 µM amino acids minus methionine (Promega), 1 µM Ipom-F, or an
339 equivalent volume of DMSO, 6.5% (v/v) ER-derived microsomes or SP cells and ~10%
340 (v/v) of *in vitro* transcribed mRNA (~500 ng/µL) encoding the relevant precursor
341 protein. Microsomal translation reactions (20 µL) were performed for 30 min at 30°C
342 whereas those using SP HeLa cells were performed on a 1.5X scale (30 µL translation
343 reactions) for 1 h at 30°C. As the S protein was most efficiently synthesised using the
344 TNT® Coupled system (Fig. S1B), import assays of the comparatively higher
345 molecular weight ACE2 and S proteins (50 µL reactions) were both performed using
346 the TNT® Coupled Transcription/ Translation system (Promega) for 90 min at 30°C as
347 described by the manufacturer (~50 ng/µL cDNA,1 µM Ipom-F or an equivalent volume
348 of DMSO, 12% (v/v) ER-derived microsomes or SP cells). All translation reactions
349 were finished by incubating with 0.1 mM puromycin for 10 min at 30°C to ensure
350 translation termination and ribosome release of newly synthesised proteins prior to
351 analysis.

352 Recovery and analysis of radiolabelled products

353 Following puromycin treatment, microsomal membrane-associated fractions were
354 recovered by centrifugation through an 80 µL high-salt cushion (0.75 M sucrose, 0.5
355 M KOAc, 5 mM $Mg(OAc)_2$, 50 mM Hepes-KOH, pH 7.9) at 100,000 ***g*** for 10 min at 4°C
356 and the pellet suspended directly in SDS sample buffer. To confirm the topology of
357 ORF6 (Fig. S2), the membrane-associated fraction of the doubly-OPG2-tagged form
358 (OPG2-ORF6-OPG2) was resuspended in KHM buffer (20 µL) and subjected to either
359 carbonate extraction (0.1 M Na_2CO_3) (McKenna et al., 2016) or a protease protection
360 assay using trypsin (1 µg/mL) with or without 0.1% Triton X-100 (Ray-Sinha et al.,
361 2009) prior to suspension in SDS sample buffer. For translation reactions using SP
362 cells, the total reaction material was diluted with nine volumes of Triton
363 immunoprecipitation buffer (10 mM Tris-HCl, 140 mM NaCl, 1 mM EDTA, 1% Triton
364 X-100, 5 mM PMSF, 1 mM methionine, pH 7.5). Samples were incubated under
365 constant agitation with an antibody recognising the OPG2 epitope (1:200 dilution) for
366 16 h at 4°C to recover both the membrane-associated and non-targeted nascent
367 chains. Samples were next incubated under constant agitation with 10% (v/v) Protein-
368 A-Sepharose beads (Genscript) for a further 2 h at 4°C before recovery by
369 centrifugation at 13,000 ***g*** for 1 min. Protein-A-Sepharose beads were washed twice
370 with Triton immunoprecipitation buffer prior to suspension in SDS sample buffer.
371 Where indicated, samples were treated with 1000 U of Endoglycosidase Hf (~10-50
372 kDa protein substrates; New England Biolabs, P0703S) or Endoglycosidase H (~50-
373 150 kDa protein substrates; New England Biolabs, P0702S), and all samples were
374 solubilised for 12 h at 37°C and then sonicated prior to resolution by SDS-PAGE (10%
375 or 16% PAGE, 120V, 120-180 min). Gels were fixed for 5 min (20% MeOH, 10%
376 AcOH), dried for 2 h at 65°C and radiolabelled products visualised using a Typhoon
377 FLA-700 (GE Healthcare) following exposure to a phosphorimaging plate for 24-72 h.
378

379 Western Blotting

380 Following semi-permeabilisation, aliquots of siRNA-treated HeLa cells were
381 suspended in SDS sample buffer, denatured for 12 h at 37°C and sonicated prior to
382 resolution by SDS-PAGE (16% or 10% PAGE, 120V, 120-150 min). Following transfer
383 to a PVDF membrane in transfer buffer (0.06 M Tris, 0.60 M glycine, 20% MeOH) at
384 300 mA for 2.5 h, PVDF membranes were incubated in 1X Casein blocking buffer (10X

385 stock from Sigma-Aldrich, B6429) made up in TBS, incubated with appropriate primary
386 antibodies (1:500 or 1:1000 dilution) and processed for fluorescence-based detection
387 as described by LI-COR Biosciences using appropriate secondary antibodies (IRDye
388 680RD Donkey anti-Goat, IRDye 680RD Donkey anti-Rabbit, IRDye 800CW Donkey
389 anti-Mouse) at 1:10,000 dilution. Signals were visualised using an Odyssey CLx
390 Imaging System (LI-COR Biosciences).
391
392 Quantification and Statistical Analysis
393 Bar graphs depict either the efficiency of membrane translocation/insertion calculated
394 as the ratio of N-glycosylated protein relative to the amount of non-N-glycosylated
395 protein (Fig. 2-3), or the efficiencies of siRNA-mediated knockdown in SP cells
396 calculated as a proportion of the protein content when compared to the NT control
397 (Fig. S2), with all control samples set to 100%. Normalised values were used for
398 statistical comparison (one-way or two-way ANOVA; DF and F values are shown in
399 each figure as appropriate and the multiple comparisons test used are indicated in the
400 appropriate figure legend). Statistical significance is given as n.s., non-significant >0.1;
401 *, $P < 0.05$; **, $P < 0.01$; ***, $P < 0.001$; ****, $P < 0.0001$.
402
403 **Acknowledgements**
404 We thank Quentin Roebuck for technical assistance, Nevan Krogan (UCSF, US) for
405 providing the original SARS-CoV-2 plasmids, Sven Lang (University of Saarland,
406 Homburg, Germany) for Sec61α antisera, Belinda Hall (University of Surrey, UK) and
407 Rachel Simmonds (University of Surrey, UK) for passing on the SARS-CoV-2 plasmids
408 and useful discussions. We are indebted to Richard Zimmermann (University of
409 Saarland) for catalyzing SARS-CoV-2 related discussions amongst the ER research
410 community and for critical feedback during the preparation of our manuscript.
411
412 **Competing interests**
413 The authors declare no competing interests.

414 **Author Contributions**

415 K.B.D., G.Z. and H.S. participated in the chemical synthesis of Ipom-F and W.Q.S
416 supervised the synthesis; P.R. subcloned and validated the SARS-CoV-2 plasmids
417 used in this study; S.O'K. performed the site-directed mutagenesis and experiments;
418 S.O'K. and S.H. designed the study, analysed the data and wrote the manuscript.

419

420 **Funding**

421 This work was supported by a Welcome Trust Investigator Award in Science
422 204957/Z/16/Z (S.H.), an AREA grant 2R15GM116032-02A1 from the National
423 Institute of General Medical Sciences of the National Institutes of Health (NIH) and a
424 Ball State University (BSU) Provost Startup Award (W.Q.S.).

425

426 **Supplementary Information**

427 Supplementary information accompanies this short report and includes Fig. S1 and
428 Fig. S2.

429 **References**

430 **Adalja, A., and Inglesby, T.** (2019). Broad-spectrum antiviral agents: A crucial
431 pandemic tool. *Exp. Rev. Anti-Infect. Ther.* **17**, 467-470.
432
433 **Bojkova, D., Klann, K., Koch, B., Widera, M., Krause, D., Ciesek, S., Cinatl, J.,**
434 **and Münch, C.** (2020). Proteomics of SARS-CoV-2 infected host cells reveals therapy
435 targets. Nature. 583, 469-472.
436
437 **Cantuti-Castelvetri, L., Ojha, R., Pedro, L. D., Djannatian, M., Franz, J., Kuivanen,**
438 **S., van der Meer, F., Kallio, K., Kaya, T., Anastasina, M., et al.** (2020). Neuropilin-
439 1 facilitates SARS-CoV-2 cell entry and infectivity. *Science.* **370**, 856-860.
440
441 **Chitwood, P. J., Juszkiewicz, S., Guna, A., Shao, S., and Hegde, R. S.** (2018).
442 EMC is required to initiate accurate membrane protein topogenesis. *Cell.* **175**, 1-13.
443
444 **Daly, J. L., Simonetti, B., Klein, K., Chen, K.-E., Kavanagh Williamson, M., Antón-**
445 **Plágaro, C., Shoemark, D. K., Simón-Gracia, L., Bauer, M. et al.** (2020). Neuropilin-
446 1 is a host factor for SARS-CoV-2 infection. *Science*. **370**, 861-865.
447
448 **Drew, E. D., and Janes, R. W.** (2020). Identification of a druggable binding pocket in
449 the spike protein reveals a key site for existing drugs potentially capable of combating
450 Covid-19 infectivity. *BMC Mol. Cell Biol.* **21**, 49.
451
452 **Duart, G., García-Murria, M. J., Grau, B., Acosta-Cáceres, J. M., Martínez-Gil, L.,**
453 **and Mingarro I.** (2020) SARS-CoV-2 envelope protein topology in eukaryotic
454 membranes. *Open Biol.* **10**, 200209.
455
456 **Firth, A. E.** (2020). A putative new SARS-CoV protein, 3c, encoded in an ORF
457 overlapping ORF3a. *J. Gen. Virol.* **101**, 1085-1089**.**
458
459 **Gérard, S. F., Hall, B. S., Zaki, A. M., Corfield, K. A., Mayerhofer, P. U., Costa, C.,**
460 **Whelligan, D. K., Biggin P. C., Simmonds, R. E., and Higgins, M. K.** (2020).
461 Structure of the inhibited state of the Sec translocon. *Mol. Cell.* **79**, 406-415.e7.

462 **Gordon, D. E., Jang, G. M., Bouhaddou, M., Xu, J., Obernier, K., White, K. M.,**
463 **O'Meara, M. J., Rezelj, V. V., Guo, J. Z., Swaney, D. L., Tummino, T. A. et al.** (2020)
464 A SARS-CoV-2 protein interaction map reveals targets for drug repurposing. *Nature.*
465 **583**, 459-468.
466
467 **Heaton, N. S., Moshkina, N., Fenouil, R., Gardner, T. J., Aguirre, S., Shah, P. S.,**
468 **Zhao, N., Manganaro, L., Hultquist, J. F., Noel, J. et al.** (2016). Targeting viral
469 proteostasis limits influenza virus, HIV, and Dengue virus infection. *Immunity.* **44**, 46-
470 58.
471
472 **Li, J.-Y., Liao, C.-H., Wang, Q., Tan, Y.-., Luo, R., Qiu, Y., and Ge, X.-Y.** (2020). The
473 ORF6, ORF8 and nucleocapsid proteins of SARS-CoV-2 inhibit type I interferon
474 signalling pathway. *Virus Res.* **286**, 198074.
475
476 **Luesch, H., and Paavilainen, V. O.** (2020). Natural products as modulators of
477 eukaryotic protein secretion. *Nat. Prod. Rep.* **37**, 717-736.
478
479 **Mast, F. D., Navare, A. T., van der Sloot, A. M., Coulombe-Huntington, J. Rout,**
480 **M. P., Baliga, N. S., Kaushansky, A., Chait, B. T., Aderem, A., Rice, C. M. et al.**
481 (2020). Crippling life support for SARS-CoV-2 and other viruses through synthetic
482 lethality. J. Cell. Biol. **219**, e202006159.
483
484 **McKenna, M., Simmonds, R.E., and High, S.** (2016). Mechanistic insights into the
485 inhibition of Sec61-dependent co- and post-translational translocation by
486 mycolactone. *J. Cell Sci.* **129**, 1404-1415.
487
488 **Morel, J. D., Paatero, A. O., Wei, J., Yewdell, J. W., Guenin-Macé, L., Van Haver,**
489 **D., Impens, F., Pietrosemoli, N., Paavilainen, V. O., and Demangel, C.** (2018).
490 Proteomics reveals scope of mycolactone-mediated Sec61 blockade and distinctive
491 stress signature. *Mol. Cell Prot.* **17**, 1750-1765.
492
493 **Naqvi, A. A. T., Fatima, K., Mohammad, T., Fatima, U., Singh, I. K., Singh, A., Atif,**
494 **A. M., Hariprasad, G., Hasan, G. M., and Hassan, M. I.** (2020) Insights into SARS-

495 CoV-2 genome, structure, evolution, pathogenesis and therapies: structural genomics
496 approach. *Biochim. Biophys. Acta. Mol. Basis Dis.* **1866**, 165878.
497
498 **Netland, J., Ferraro, D., Pewe, L., Olivares, H., Gallagher, T., and Perlman, S.**
499 (2007). Enhancement of murine coronavirus replication by severe acute respiratory
500 syndrome coronavirus protein 6 requires the N-terminal hydrophobic region but not C-
501 terminal sorting motifs. *J. Virol.* **81**, 11520-11525.
502
503 **Nilsson, I. M., and von Heijne, G.** (1993). Determination of the distance between the
504 oligosaccharyltransferase active site and the endoplasmic reticulum membrane. *J.*
505 *Biol. Chem.* **268**, 5798-5801.
506
507 **Ray-Sinha, A., Cross, B. C. S., Mironov, A., Wiertz, E., and High, S.** (2009).
508 Endoplasmic reticulum-associated degradation of a degron-containing polytopic
509 membrane protein. *Mol. Membr. Biol.* **26**, 448-464.
510
511 **O'Keefe, S., Zong, G., Duah, K. B., Andrews, L. E., Shi, W. Q., and High, S.** (2020).
512 Type III transmembrane protein integration requires both the EMC and Sec61
513 complex. Submitted.
514
515 **Sicari, D., Chatziioannou, A., Koutsandreas, T., Sitia, R., and Chevet, E.** (2020).
516 Role of the early secretory pathway in SARS-CoV-2 infection. *J. Cell. Biol.* **219**,
517 e202006005.
518
519 **Shah, P. S., Link, N., Jang, G. M., Sharp, P. P., Zhu, T., Swaney, D. L., Johnson,**
520 **J. R., Von Dollen, J., Ramage, H. R., Satkamp, L. et al.** (2018). Comparative
521 flavivirus-host protein interaction mapping reveals mechanisms of Dengue and Zika
522 virus pathogenesis. *Cell.* **175**, 1931-1945.e18.
523
524 **Von Heijne, G.** (2007). The membrane protein universe: what's out there and why
525 bother? *J. Intern. Med.* **261**, 543-547.
526

527 **Walls, A. C., Park, Y.-J., Tortorici, M. A., Wall, A., McGuire, A. T., and Veesler, D.**
528 (2020). Structure, function and antigenicity of the SARS-CoV-2 spike glycoprotein.
529 *Cell.* **181**, P281-292.E6.
530
531 **Warner, F. J., Lew, R. A., Smith, A. I., Lambert, D. W., Hooper, N. M., and Turner,**
532 **A. T.** (2005). Angiotensin-converting enzyme 2 (ACE2), but not ACE, is preferentially
533 localised to the apical surface of polarised kidney cells. *J. Biol. Chem.* **280**, 39353-
534 39362.
535
536 **Wilson, C. M., and High, S.** (2007). Ribophorin I acts as a substrate-specific facilitator
537 of N-glycosylation. *J. Cell. Sci.* **120**, 648-657.
538
539 **Young, B. E., Fong, S.-W., Chan, Y. H., Mak, T.-M., Ang, L. W., Anderson, D. E.,**
540 **Yi-Pin Lee, C., Naqiah Amrun, S., Lee, B., Shan Goh, Y. et al.** (2020). Effects of a
541 major deletion in the SARS-CoV-2 genome on the severity of infection and
542 inflammatory response: an observational cohort study. *Lancet.* **396**, 603-611.
543
544 **Zhang, Y., Zhang, J., Chen. Y., Luo, B., Yuan, Y., Huang, F., Yang, T., Yu, F., Liu,**
545 **J., Song, Z. et al.** (2020). The ORF8 protein of SARS-CoV-2 mediates immune
546 evasion through potently downregulating MHC-1. bioRxiv.
547 **doi:** 10.1101/2020.05.24.111823
548
549 **Zhou, P., Yang, X.-L., Wang, X.-G., Hu, B., Zhang, L., Zhang, W., Si, H.-R., Zhu,**
550 **Y., Li, B., Huang, C.-L. et al.** (2020). A pneumonia outbreak associated with a new
551 coronavirus of probable bat origin. *Nature.* **579**, 270-273.
552
553 **Zhu, N., Zhang, D., Wang, W., Li, X., Yang, B., Song, J., Zhao, X., Huang, B., Shi,**
554 **W., Lu, R., et al.** (2020). A novel coronavirus from patients with pneumonia in China,
555 2019. *N. Eng. J. Med.* **382**, 727-733.
556
557 **Zong, G., Hu, Z., O'Keefe, S., Tranter, D., Iannotti, M. J., Baron, L., Hall, B.,**
558 **Corfield, K., Paatero, A., Henderson M. et al.** (2019). Ipomoeassin F binds Sec61α
559 to inhibit protein translocation. *J. Am. Chem. Soc.* **141**, 8450-8461.

560 **Zong, G., Hu, Z., Duah, K., B., Andrews, L. E., Zhou, J., O'Keefe, S., Whisenhunt,**
561 **L., Shim, J. S., Du, Y., High, S., et al.** (2020) Ring-expansion leads to a more potent
562 analogue of ipomoeassin F. *J. Org. Chem.* In press.

Supplementary information for

Ipomoeassin-F inhibits the *in vitro* biogenesis of the SARS-CoV-2 spike protein and its host cell membrane receptor

Sarah O'Keefe, Peristera Roboti, Kwabena B. Duah, Guanghui Zong, Hayden Scheider, Wei Q. Shi and Stephen High

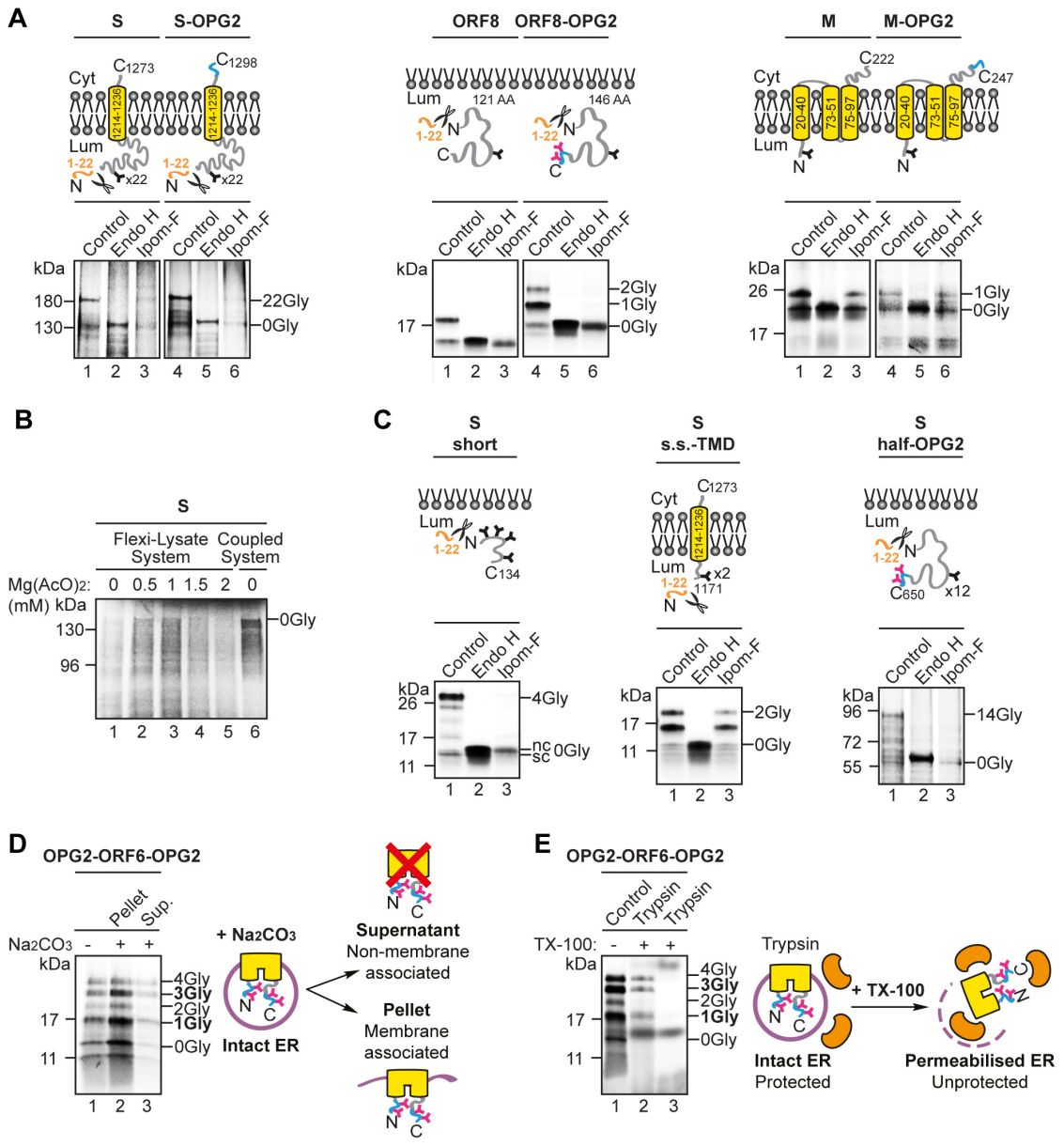

Fig. S1. Additional studies using ER microsomes, Related to Figures 2 and 3. (**A**) Non-tagged (lanes 1-3) and OPG2-tagged (lanes 4-6) versions of the SARS-CoV-2 spike protein (S, S-OPG2), ORF8 (ORF8, ORF8-OPG2) and membrane protein (M, M-OPG2) were synthesised in rabbit reticulocyte lysate supplemented with ER-derived canine pancreatic microsomes in the absence and presence of Ipom-F (lanes 1 and 3). Phosphorimages of membrane-associated products resolved by SDS-PAGE together with representative substrate outlines are shown. N-glycosylated (X-Gly) versus non-N-glycosylated (0Gly) species were identified by treatment with endoglycosidase H (Endo H, lanes 2 and 5). (**B**) The S protein was synthesised in a Flexi® rabbit reticulocyte system with varying concentrations of magnesium acetate (lanes 1-5) and a TNT® Coupled system (lane 6) in the absence of ER-derived

microsomes. 5% of the total reaction material was resolved by SDS-PAGE and visualised by phosphorimaging. (**C**) The ER import of truncated variants of the S protein (S-short, S-s.s.-TMD, S-half-OPG2) was analysed as described for **(A)**. (**D**) The membrane-associated products of the doubly tagged form of ORF6 (OPG2-ORF6-OPG2) were synthesised as in **(A)** and, following treatment with sodium carbonate buffer and centrifugation, the pellet, enriched for membrane-integrated material, and supernatant, largely containing peripherally membrane-associated material, were analysed for OPG2-ORF6-OPG2. (**E**) The membrane-associated products of OPG2-ORF6-OPG2 were treated with trypsin in the absence or presence of Triton-100 (TX-100, lanes 2-3).

563

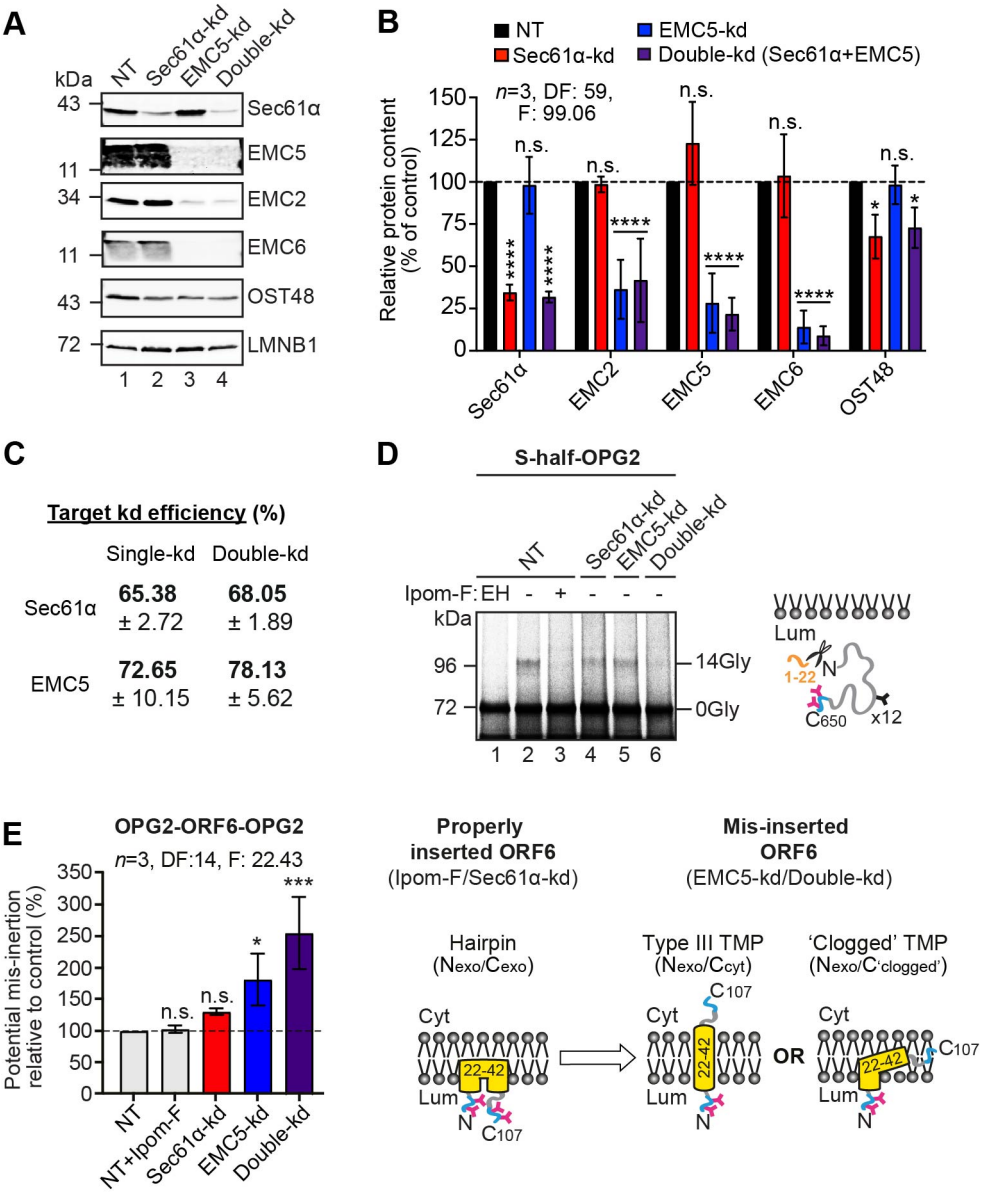

Fig. S2. Validation of Sec61 and/or EMC subunit depletions in SP cells, Related to Figure 3.

(A) The effects of transfecting HeLa cells with non-targeting (NT; lane 1), Sec61α-targeting (lane 2), EMC5-targeting (lane 3) and Sec61α+EMC5-targeting (lane 4) siRNAs were determined after semi-permeabilisation by immunoblotting for target genes (Sec61α, EMC5). Controls to assess destabilisation of the wider EMC complex (EMC2 and EMC6), any effect on the N-glycosylation machinery (the ER-resident 48 kDa subunit of the oligosaccharyl-transferase complex (OST48) and the quantity of SP cells used in each experiment (the nuclear protein Lamin-B1 (LMNB1)), are also shown. (**B**) The efficiencies of siRNA-mediated knockdown (bold) were calculated as a proportion of the signal intensity obtained with the NT control (set as 100%).

Quantifications are given as means ±SEM for three separate siRNA treatments (*n*=3) with statistical significance of siRNA-mediated knockdowns (two-way ANOVA, DF and F values shown in the figure) determined using Dunnett's multiple comparisons test. Statistical significance is given as n.s., non-significant >0.1; *, P < 0.05; ****, P < 0.0001. (**C**) Mean knockdown efficiencies (±SEM) for each of the target genes. (**D**) A truncated variant of the S protein (S-half-OPG2) was synthesised in rabbit reticulocyte lysate supplemented with SP cells with impaired Sec61 complex and/or EMC function and recovered by immunoprecipitation via the OPG2 tag. Radiolabelled products resolved by SDS-PAGE and analysed by phosphorimaging. N-glycosylated (14-Gly) versus non-N-glycosylated (0Gly) species were identified by treatment with endoglycosidase H (Endo H, lane 1). (**E**) Further analysis of the data presented in Fig. 3E of the main text. Here, the ratio of 3Gly and 4Gly bearing OPG2-ORF6-OPG2 N-glycosylated species relative to the 1Gly species present in the same sample was used as a proxy to estimate potential mis-insertion of the ORF6 protein in SP cells with impaired Sec61 complex and/or EMC function relative to the NT control (set to 100% efficiency). Quantifications are given as means ±SEM for independent translation reactions from separate siRNA treatments performed in triplicate (*n*=3) and statistical significance (two-way ANOVA, DF and F values shown in the figure) was determined using Dunnett's multiple comparisons test. Statistical significance is given as n.s., non-significant >0.1; *, P < 0.05; ***, P < 0.001.